Nonlinear wave interaction with bottom-mounted structures by a high-order Boussinesq method

H.B. Bingham[*], D.R. Fuhrman[*], E. Jamois[†] and O. Kimmoun[†]

Abstract. This paper reports on our first attempts to compute highly-nonlinear wave interaction with bottom-mounted coastal structures using a high-order Boussinesq method. The results presented here include the classical linear diffraction pattern around a breakwater (for validation), and the nonlinear interaction of waves with a bottom-mounted plate where we compare to the experimental measurements discussed by Molin *et al.* [1] at the 18$^{\text{th}}$ workshop. The computed results involving linear breakwater diffraction, while not perfect, are in reasonable agreement with the theoretical predictions. More impressively, a highly-nonlinear simulation involving run-up on a vertical plate is in excellent agreement with experimental measurements.

1 The Boussinesq model

The Boussinesq method used to make these computations is derived in [2, 3], where it is shown to accurately propagate nonlinear traveling waves in dimensionless water depths up to $kh \approx 25$ (k the wavenumber, h the water depth) right up to the stable breaking limit. The associated wave kinematics (vertical distribution of pressure and velocity) are accurate up to $kh \approx 12$. In [6] the method has been used to investigate three-dimensional instabilities leading to crescent wave patterns of extreme nonlinearity. To briefly outline the method, we consider water waves in three-dimensions using a coordinate system having the origin on the still-water plane, with the z-axis pointing vertically upwards. The fluid domain is bounded by the sea bed at $z = -h(\mathbf{x})$, with $\mathbf{x} = [x, y]$, and the free surface at $z = \eta(\mathbf{x}, t)$, where t is time. The free surface boundary conditions are written in terms of velocity components at the free surface $\tilde{\mathbf{u}} = [\tilde{u}, \tilde{v}] = \mathbf{u}(\mathbf{x}, \eta, t)$ and $\tilde{w} = w(\mathbf{x}, \eta, t)$:

$$\frac{\partial \eta}{\partial t} = \quad \tilde{w}\left(1 + \nabla\eta \cdot \nabla\eta\right) - \tilde{\mathbf{U}} \cdot \nabla\eta, \tag{1}$$

$$\frac{\partial \tilde{\mathbf{U}}}{\partial t} = \quad -g\nabla\eta - \frac{1}{2}\nabla\left(\tilde{\mathbf{U}} \cdot \tilde{\mathbf{U}} - \tilde{w}^2\left(1 + \nabla\eta \cdot \nabla\eta\right)\right), \tag{2}$$

where $\nabla = [\partial/\partial x, \partial/\partial y]$ is the 2-D gradient operator and $\tilde{\mathbf{U}} = [\tilde{U}, \tilde{V}] = \tilde{\mathbf{u}} + \tilde{w}\nabla\eta$. Evolving η and $\tilde{\mathbf{U}}$ forward in time requires a means of computing $\tilde{w}$ subject to the Laplace equation and the kinematic bottom condition (KBC): $w + \nabla h \cdot \mathbf{u} = 0$ (at $z = -h$). A highly-accurate Boussinesq method for this purpose is obtained by approximating the vertical distribution of fluid velocity by

$$\mathbf{u}(\mathbf{x}, z, t) = (1 - \alpha_2\nabla^2 + \alpha_4\nabla^4)\hat{\mathbf{u}}^*(\mathbf{x}, t) + ((z - \hat{z})\nabla - \beta_3\nabla^3 + \beta_5\nabla^5)\hat{w}^*(\mathbf{x}, t), \tag{3}$$

$$w(\mathbf{x}, z, t) = (1 - \alpha_2\nabla^2 + \alpha_4\nabla^4)\hat{w}^*(\mathbf{x}, t) - ((z - \hat{z})\nabla - \beta_3\nabla^3 + \beta_5\nabla^5)\hat{\mathbf{u}}^*(\mathbf{x}, t), \tag{4}$$

where $\alpha_2 = \frac{(z-\hat{z})^2}{2} - \frac{\hat{z}^2}{18}$, $\alpha_4 = \frac{(z-\hat{z})^4}{24} - \frac{\hat{z}^2(z-\hat{z})^2}{36} + \frac{\hat{z}^4}{504}$, $\beta_3 = \frac{(z-\hat{z})^3}{6} - \frac{\hat{z}^2(z-\hat{z})}{18}$, and $\beta_5 = \frac{(z-\hat{z})^5}{120} - \frac{\hat{z}^2(z-\hat{z})^3}{108} + \frac{\hat{z}^4(z-\hat{z})}{504}$. In (3) and (4) the quantities $\hat{\mathbf{u}}^*$ and $\hat{w}^*$ are utility variables which have been introduced to allow Padé enhancement of the Taylor series operators. Optimal velocity distributions are obtained near $\hat{z} = -h/2$, and we adopt this value here. Inserting (3) and (4) into the KBC gives one equation relating $\hat{\mathbf{u}}^*$ and $\hat{w}^*$ to each other. Combining this with (3) applied at $z = \eta$, while also invoking the definition of $\tilde{\mathbf{U}}$, gives a 3×3 system that can be solved for

[*]Mechanical Eng., Technical University of Denmark. Contact: hbb@mek.dtu.dk
[†]Hydrodynamics Dept., Ecole Supérieure d'Ingénieurs de Marseille, France.

$\hat{\mathbf{u}}^*$ and $\hat{w}^*$ in terms of $\tilde{\mathbf{U}}$ and η. More complete details on the basic finite difference model can be found in [4], and we use the irrotational version described therein. This reference explores a number of effective preconditioning strategies which allow a solution effort which scales very nearly with N, the number of grid points distributed over a horizontal plane. The stability of the resulting numerical method is further considered in [5]. Throughout this work we use the classical fourth-order, four-stage explicit Runge-Kutta time-stepping scheme.

To include bottom-mounted fixed structures into the existing Boussinesq model is conceptually trivial, but introduces several practical problems. It is well known that the potential flow solution around an exterior corner is singular, predicting infinite velocity around the corner. The singularity is rather weak however (proportional to $1/r^{1/3}$ in an infinite fluid) and one could argue that it has no physical significance since viscosity and finite curvature effects will always make the velocities finite in reality. In this spirit, we take an approach of not trying to "over-resolve" the flow near a corner by simply defining the location of the structure to lie half way between grid points. See Figure 1.

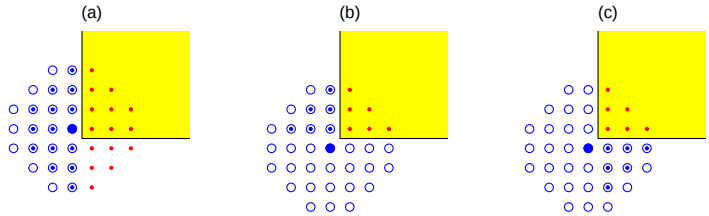

Figure 1: Placement of structures within the computational grid showing the treatments of mixed-derivatives near an exterior corner. The shaded region is the structure, the center-point is given by $\bullet$, coefficients reflected across the walls are denoted $\cdot$ and land on the $\odot$ points. (a) shows the pattern taking the $y-$derivative first for a center-point adjacent to a vertical (in plan) wall. (b) & (c) show potential stencils for a center-point not adjacent to a wall, when first taking the x- and y-derivatives, respectively.

This figure also illustrates a second problem which concerns the treatment of mixed-derivatives at points whose finite difference stencil overlaps an exterior corner. Figure 1 demonstrates this for the 37-point stencil used throughout the present work. Wall conditions are imposed by reflecting all coefficients which land outside of the fluid domain across the walls, under the assumption that the function being operated on is either even or odd with respect to the boundary. Mixed x- and y-derivatives have two obvious representations near a corner, which can be thought of conceptually as taking the x-derivatives at all stencil points lying along the centerline in y, and then using this result to take the remaining y-derivatives at the center-point; or the reverse. Since the continuous derivative may be taken in either order, both of these approximations are formally consistent, but they lead to different schemes having different symmetries about the corner. Three examples are shown in Figure 1. As shown in Figure 1 (a), for center-points adjacent to a wall we first conceptually take derivatives in the direction parallel to the wall, with the remaining derivatives operating on these values. For points neighboring an exterior corner that are not adjacent to a wall, we use a combination of the two possibilities shown *e.g.* in Figures 1 (b) and (c), which can conceptually be thought as

$$\frac{\partial^{j+k}}{\partial x^j \partial y^k} = \frac{1}{2}\frac{\partial^j}{\partial x^j}\left(\frac{\partial^k}{\partial y^k}\right) + \frac{1}{2}\frac{\partial^k}{\partial y^k}\left(\frac{\partial^j}{\partial x^j}\right). \tag{5}$$

This approach conveniently leads to discretizations that are symmetric about the corner.

Both analysis and experience has shown that the resulting discretizations are prone to mild linear instabilities (due to taking high-order derivatives around exterior corner points). Steep velocity gradients are also typically present around these corners, which lead to numerical inaccuracies and convergence problems. These tend to produce high-frequency noise, which can also

quickly excite nonlinear instabilities, or pollute the rest of the domain. To combat these problems, we employ a sixth-order, 57-point (octagon shaped) Savitzky-Golay smoothing filter. Throughout most of the domain this is applied incrementally after full time steps. Alternatively, around structures we use a simpler version (summing the coefficients first along an x-, and then a y-line), applied after each Runge-Kutta stage, sometimes repeatedly.

2 Test cases

We now present results from two numerical simulations with the Boussinesq model involving wave interaction with bottom-mounted structures. All cases are discretized using $\Delta x \approx \Delta y \approx L/20$ with $\Delta t = T/20$. We use a wavemaker relaxed over a distance consisting of a single wavelength, with a similar relaxation zone at the opposing end to absorb the outgoing wave field.

The first case involves linear diffraction around a semi-infinite breakwater. We consider linear waves with $kh = \pi/2$ propagating in the $+y$-direction on a 400×221 computational domain (the domain is taken to be wide enough to avoid significant reflection from the side-walls over the simulated time). A structure is placed covering the right-half of the domain, extending half a grid point beyond the wavemaker in the y-direction. The origin is placed at the corner location. The computed and theoretical diffraction diagrams are shown in Figure 2. The results are clearly not perfect, but are reasonable. Most notably, there is an underestimation of the wave heights in the shadow zone. The overall error in fact radiates quite regularly from the corner-point, however, and the accuracy is likely sufficient for engineering purposes. A simulation with $kh = 2\pi$ results in a diffraction diagram having similar quality, with better agreement in the shadow zone, but a slight increase in the error in the negative x-region. This will also be presented at the workshop.

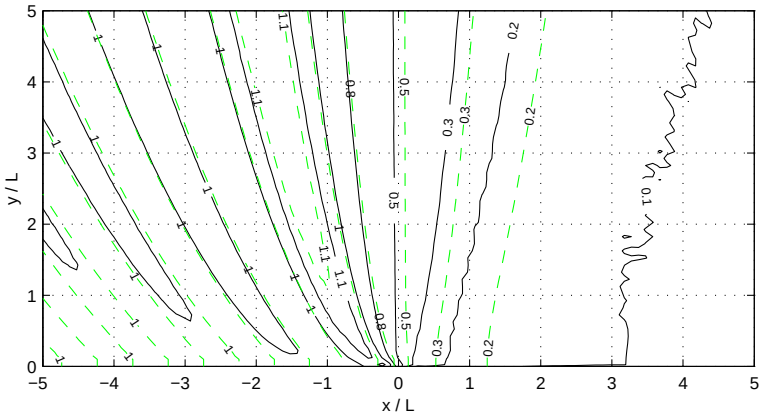

Figure 2: Computed (solid) and theoretical (dashed) linear diffraction diagrams with $kh = \pi/2$.

We finally present computational results involving deep-water wave run-up on a plate (due to third-order effects) described at the 18th workshop in [1]. In the physical experiments a vertical 1.2 m bottom-mounted plate is projected from the sidewall a distance of 19.3 m from the wavemaker in a 16 m wide, 3 m deep wave-tank (our simulations use a 383×201 computational domain, with a smaller width of 12.3 m to ease the computational burden). We consider the case with $H = 0.046$ m, $T = 0.88$ s and reduce the depth to $h = 0.6$ m. We use stream function incident waves propagating in the $+x$-direction, giving a wavelength $L = 1.22$ m ($kh \approx \pi$, $H/L = 0.038$). Computed envelopes (taken over $55 < t < 60$ s) along the front of the plate, as well as along $y = 0$ are shown in Figures 3 and 4, respectively. The match with the measurements in Figure 3 is excellent. Comparisons with the measured time series are equally impressive on both sides of the plate, matching the relative phase and amplitude very well. Note the extreme nonlinearities involved; a maximum steepness of $H/L \approx 0.131$ is observed a distance of $L/2$ in front of the plate in Figure 4.

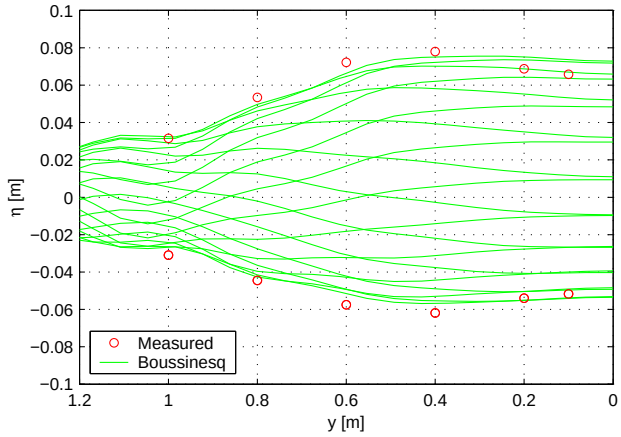

Figure 3: Computed and measured free surface envelope in front of the plate.

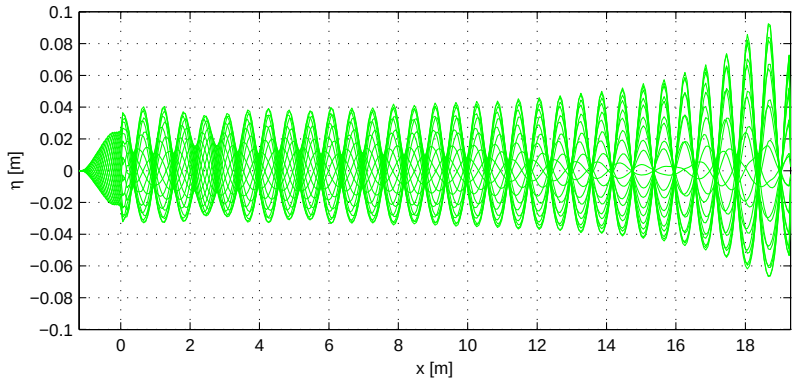

Figure 4: Computed free surface envelope along $y = 0$.

This work was supported by the Danish National Research Council (STVF grant no. 9801635). Their support is greatly appreciated.

References

[1] Molin, B., F. Remy, O. Kimmoun, and P. Ferrant. Third-order interactions and wave run-up. *Proc. 18th Int. Workshop on Water Waves and Floating Bodies.* Le Croisic, France, 2003.

[2] Madsen, P.A., H.B. Bingham, and H.A. Schäffer. Boussinesq-type formulations for fully nonlinear and extremely dispersive water waves: Derivation and analysis. *Proc. Roy. Soc. Lond. A* **459**, 1075–1104, 2003.

[3] Madsen, P.A., H.B. Bingham, and H. Liu. A new Boussinesq method for fully nonlinear waves from shallow to deep water. *J. Fluid Mech.* **462** 1–30, 2002.

[4] Fuhrman, D.R. and H.B. Bingham. Numerical solutions of fully nonlinear and highly dispersive Boussinesq equations in two horizontal dimensions. *Int. J. Numer. Meth. Fluids*, In press.

[5] Fuhrman, D.R., H.B. Bingham, P.A. Madsen, and P.G. Thomsen. Linear and nonlinear stability analysis for finite difference discretizations of high-order Boussinesq equations. Submitted to *Int. J. Numer. Meth. Fluids*, 2003.

[6] Fuhrman, D.R., P.A. Madsen, and H.B. Bingham. A numerical study of crescent waves. Submitted to *J. Fluid Mech.*, 2003.